Journal of Materials Chemistry

Cite this: *J. Mater. Chem.*, 2012, **22**, 3745

www.rsc.org/materials

PAPER

Soft lithographic patterning of spin crossover complexes. Part 1: fluorescent detection of the spin transition in single nano-objects†

Carlos M. Quintero,[a] Il'ya A. Gural'skiy,[ab] Lionel Salmon,[a] Gábor Molnár,*[a] Christian Bergaud[c] and Azzedine Bousseksou*[a]

Received 4th November 2011, Accepted 12th December 2011
DOI: 10.1039/c2jm15662h

The investigation of size-reduction effects on the spin crossover properties of a class of transition metal complexes has recently become an area of intensive research. However, to avoid inter-particle interactions, ensemble averaging and matrix effects it is necessary to develop methods for the systematic study of individual nano-objects. To this aim thin films and nano-patterns of the compound $[Fe^{II}(hptrz)_3](OTs)_2$ doped with acridine orange were elaborated by spin coating and soft-lithography, respectively. The luminescence intensity was found to change significantly upon the spin transition even in isolated nano-objects of *ca.* 150 nm size, allowing us to monitor in a massively parallel way the spin crossover phenomenon in large arrays *via* fluorescence microscopy.

Introduction

In contrast to semiconductors and metals, size effects in molecular materials have remained largely unexplored—probably due to the lack of electron confinement effects.[1] Nevertheless, the increase of surface energy, elastic confinement and loss of translational symmetry have led to profound changes in molecular nano-objects as well. In this context, the recent emergence of spin crossover (SCO) nano-materials provides an excellent platform to investigate size reduction effects in molecular solids owing to the extreme sensitivity of the SCO phenomenon to minute changes in the crystal lattice. Spin crossover between the high spin (HS) and low spin (LS) electronic configurations was reported in a number of $3d^4$–$3d^7$ transition metal complexes.[2] The switching between the two spin states is accompanied by a significant change of molecular shape and volume leading to strong elastic interactions between the molecules in most bulk solids. These cooperative intermolecular interactions associated with the small energy gap between the HS and LS states are expected to give rise to significant size reduction effects on the SCO phenomenon. Indeed, the study of nano-objects with SCO properties has recently become an area of intensive research.[3] Several interesting fundamental aspects such as the size effect on the spin transition temperature and on the hysteresis width as well as on the kinetics of the associated nucleation and growth phenomena are intensively studied these days. Beyond their fundamental interest, these SCO nano-materials can also respond to technological needs in sensor applications (thermometry, gas sensing), display elements, pigments, *etc.*

Up to now, the SCO nano-materials have been studied by various methods such as magnetometry or optical absorption measurements. However, these methods probe a significant ensemble of objects with different size, shape, composition, *etc.* In order to avoid these averaging effects, it is crucial to develop precise characterization methods for single particles down to the nanoscale where conventional methods are no longer effective. The aim is to correlate accurately the SCO properties with the morphology of the objects. So far, contributions towards single SCO element measurements remain scarce.[4–6] Molnár *et al.*[4] used Raman microspectroscopy to investigate nano-patterned thin films, while Arnaud *et al.*[5] employed a differential interference microscopy setup for studying single microparticles and to correlate their thermal SCO response with their size. On the other hand, the authors in ref. 6 have observed bistability and hysteresis as a function of temperature, possibly associated with SCO, in the conductance of nanoparticles placed between nano-spaced Au electrodes. Despite these promising efforts, one challenge yet to overcome in order to establish systematic characterization of nano-objects is the stochastic nature of the assemblage of the material into their substrates. Furthermore, it is difficult to assess whether these methods will be sufficiently generic and sensitive to study a variety of SCO complexes. In this paper, we propose a novel approach to solve these two problems. We use soft-lithography to organize the SCO nano-objects in a well defined array and fluorescent doping to follow the spin state change.

[a]*LCC, CNRS & Université de Toulouse (UPS, INP), 205 route de Narbonne, 31077 Toulouse, France. E-mail: gabor.molnar@lcc-toulouse.fr; azzedine.bousseksou@lcc-toulouse.fr*
[b]*Department of Chemistry, National Taras Shevchenko University, 62 Vladimirska str., 01601 Kiev, Ukraine*
[c]*LAAS, CNRS & Université de Toulouse (UPS, INSA, IAES), 7 avenue du colonel Roche, 31077 Toulouse, France*

† Electronic supplementary information (ESI) available: Dark field and AFM images of different nano-patterns and thin films of the complex $[Fe(hptrz)_3](OTs)_2$. Luminescence spectra of acridine orange. Spin transition curve of the bulk complex. Absorption spectra of the films. Spin transition curves of a series of nano-objects. See DOI: 10.1039/c2jm15662h

Under appropriate conditions, fluorescence can constitute a very sensitive method (down to single molecule detection[7]) that can render high contrast to the surroundings of the probe and as a result, higher signal-to-noise ratios can be achieved. If the emission and/or excitation spectra of a luminophore exhibit an appropriate overlap with the characteristic HS *or* LS absorption bands of the SCO material, the latter can act as a quencher depending on its spin state.[8–10] In order to enhance the quenching effect of the SCO complex and reach higher modulation of the luminescence intensity even at the scale of a single nano-object, a radiationless energy transfer between the luminophore and the Fe(II) ions is needed. To accomplish this it is imperative to achieve a short distance (~1 to 3 nm) between the luminophore and the quencher.[11] Thus, in addition to a good spectral overlap, luminophores that can approach the metallic center or even enter into its coordination sphere are needed. Further requirements include low photobleaching and—for the investigation of thermally induced SCO—a weak temperature dependence of the luminescence.

For the present work, we have selected the triazole derivative complex $[Fe(hptrz)_3](OTs)_2$ (**1**) (where *hptrz* = 4-heptyl-1,2,4-triazole and OTs = tosylate) as a SCO compound (Scheme 1). This coordination polymer is suggested to be composed of 1D "polymeric" chains of triazole-bridged Fe(II) ions with tosylate anions and water molecules situated between the chains.[12,13] We have found that nano-objects based on this complex are convenient objects for the study of size-dependent SCO phenomena due to their stability and the presence of a hysteresis. For the luminescent agent, we have chosen acridine orange (Scheme 1). This luminophore is fairly robust and its emission band has a good overlap with a LS absorption band of our complex. This paper will focus on the fluorescent detection of the thermal SCO phenomenon in **1** doped with acridine orange in two kinds of samples: spin coated thin films and single SCO nano-objects patterned *via* soft lithography methods.

Experimental

Fabrication of thin films of $[Fe(hptrz)_3](OTs)_2$

All the chemicals and solvents were obtained from Sigma Aldrich and used without any further purification. 4-Heptyl-1,2,4-triazole was prepared from 1-heptylamine, triethyl orthoformate and *N*-formylhydrazine following the procedure described previously by Bayer *et al.*[14] Iron(II) tosylate was synthesized by reaction between metallic iron and *p*-toluenesulfonic acid.[15] The mother solution of the complex was prepared by mixing two solutions; the first containing iron(II) tosylate hexahydrate (30 mg, 0.06 mmol, 1 equiv.) and *p*-toluenesulfonic acid monohydrate (4 mg, 0.02 mmol) in MeOH (150 μl) and the second containing 4-heptyl-1,2,4-triazole (60 mg, 0.36 mmol, 2 equiv.) in $CHCl_3$ (4 ml). For spin coating 50 μl of the mother solution of the complex was mixed with 0.66 mM chloroform solution of acridine orange (5 μl). The parameters set for the spin coater were: speed = 5000 rpm, acceleration = 4000 rpm^2, and time = 30 s. Note also that for the nanopatterning, an acridine orange chloroform solution (0.04 mM) was mixed with the mother solution of the complex (3 : 1 ≈ 0.8 mol% acridine orange per iron atom).

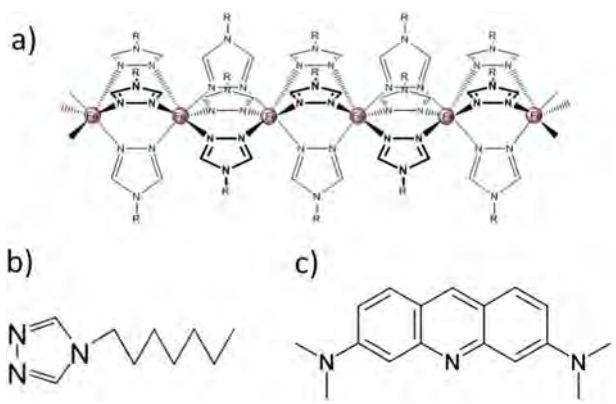

Scheme 1 (a) Schematic chain structure of the triazole family complexes,[13] (b) *hptrz* = 4-heptyl-1,2,4-triazole, and (c) acridine orange molecule.

Fabrication of PDMS stamps

The silicon master was produced by means of electron beam lithography and deep reactive ion etching (RIE). Arrays of squares with different widths (370, 350, 300 and 250 nm) and different pitches (1.5, 2, 3 and 5 μm, see Fig. S1 in the ESI†) were created in a conventional poly(methyl-methacrylate) (PMMA) resist. Then, after a Ti metallization and a lift-off process, the patterns were transferred onto the substrate *via* RIE with a nominal etch depth set to 150 nm. Additionally, to enable the demolding from this master, an antiadhesive treatment following a well-established process using octadecyltrichlorosilane was carried out.[16] After this, a solution of polydimethylsiloxane (PDMS) prepolymer (containing a mixture in a 10 : 1 mass ratio of PDMS oligomer and a reticular agent) was cured on the silicon master. Finally, the stamps were cut into 1 cm × 1 cm pieces.

Physical measurements

Fluorescence microscopy images have been recorded with an Olympus BX51 microscope equipped with an iKon-M DU934N-BV (Andor Technology) charge-coupled device (CCD) image sensor (1024 × 1024 pixels of 13 μm size) and a ×5 magnification objective (numerical aperture, $NA = 0.1$) or a ×50 magnification objective ($NA = 0.5$). The excitation and collected light beams were separated by a dichroic mirror (cutting edge at 510 nm) and they were further cleaned with band-pass filters centered at 450 nm (full width at half maximum, FWHM = 45 nm) and at 550 nm (FWHM = 50 nm), respectively. In reflectance microscopy measurements for undoped samples, the collected light beam was filtered with a band-pass filter centered at 543 nm (FWHM = 23 nm). All experiments were carried out inside the chamber of a THMS-600 Linkam cryostat and all samples were first dehydrated under nitrogen atmosphere at 353 K for 30 minutes. Variable temperature UV-vis absorption spectra were recorded on a Cary-50 (Varian) spectrophotometer on solution samples held in a thermostatted quartz cuvette. A Fluoromax-4 (Horiba Jobin Yvon) spectrofluorimeter was used to acquire fluorescence excitation and emission spectra at room temperature (RT), which were corrected for the instrument response (as implemented in the software). Raman spectra were acquired at RT using a Lab-RAM-HR (Horiba-Jobin Yvon) microspectrometer (632.8 nm

excitation). IR spectra were recorded with a Perkin Elmer Spectrum 100 spectrometer at RT either in transmission or in attenuated total reflectance (ATR) mode. Surface topographical characterization of the samples was performed under ambient conditions using a Digital Instruments Multimode Nanoscope IIIa atomic force microscope (AFM) operating in tapping mode. Scanning electron microscope (SEM) images were acquired employing a Hitachi S4800 microscope with an accelerating voltage of 30 kV.

Results and discussion

Thin films

There has been a lot of effort in the development of techniques for the organization of various molecular materials at small scales.[17,18] In the case of SCO thin films, our team has employed synthesis techniques involving sequential assembly;[4,19] others have also proposed thin films in the form of liquid-crystals,[20] lipophobic supramolecular complexes[21] and "metallo-grids".[22] The preparation of thin films by spin- or dip-coating diverse SCO complexes has also been explored.[23–26] In particular, deposition of surfactant or polymer stabilized SCO nanoparticles seemed to be a promising approach for these purposes; however, it results in the preparation of films consisting of strongly diluted SCO materials. Additionally, in certain configurations we have observed the degradation of the complex under the influence of the surfactant when the mixture was heated. To overcome these problems, we developed recently a new method by preparing a stable and homogeneous chloroform solution of $Fe(OTs)_2$ with *hptrz*.[27] This solution is thought to contain the $[Fe(hptrz)_3](OTs)_2$ complex with a low polymerization degree, but when the solvent is evaporated longer chains might be formed. The important point to notice is that this method leads to a solid which is composed primarily of the SCO compound without the presence of surfactants or any other additives.

A fresh chloroform solution of the complex was prepared and mixed with acridine orange (0.1 mol%). As a first step for characterizing the luminescent response of this system at the nanoscale, a few μl of the solution was spin coated over clean pieces of Si wafer as well as on quartz substrates. Thin and homogeneous films were obtained even on large (3×3 cm^2) substrate surfaces. These samples were observed with an AFM and an average thickness of 85 nm was measured for different samples with the same conditions of deposition. The chemical composition of the films was verified by means of Raman and infrared spectroscopies (Fig. 1). At this point we would like to emphasize the absence of additives during the deposition process; there are also no constraints concerning the nature of the substrate employed or the functionalization of its surface. Furthermore, by changing the parameters of the coater or the concentration of the reagents in the starting solution, different film thicknesses (see Fig. S2†) can be easily obtained over large surfaces and without any strong variation in the composition of the film.

The thermal response of the thin layers was monitored *via* fluorescence microscopy. The luminescence intensity was followed at 550 nm due to the perfect overlap at this wavelength between the $^1A_1 \rightarrow {}^1T_1$ absorption band of the complex and the emission spectrum of the acridine orange (excited at 450 nm) (Fig. 2a and S3†). The samples were cycled several times at a rate of 2 K min^{-1} between 253 and 353 K. As observed in Fig. 2b, between 293 and 323 K the luminescence intensity changes in an abrupt manner while heating or cooling and also a small hysteresis can be depicted within the same temperature range. Clearly this behavior is opposite to the ordinary thermal extinction of the luminescence and should be associated with the dis/re-appearance of the singlet absorption band of the complex while the $^1A \leftrightarrow {}^5T$ spin crossover phenomenon takes place. As a consequence, a modulation of the luminescence is obtained and the transition curve is in reasonable agreement with the reflectance measurements of the same undoped compound in bulk powder form (see Fig. S4†). Additionally, these experiments show that the cycles are rather reproducible and in spite of the constant excitation no photobleaching was observed.

Even if we have no precise structural information concerning the localization of the luminophore molecules in the network, the mechanism responsible for quenching the luminescence can be attributed essentially to a non-radiative transfer between the acridine orange and the Fe^{II} ions present in the complex. This hypothesis corroborates the increase of ~50% of the signal during the transition. Indeed, given the thickness of our films (85 nm) and the variation of the molar absorption coefficient (ε) of this complex during the SCO at the selected excitation and emission wavelengths of the luminophore ($\Delta\varepsilon \approx 7.5$ L mol^{-1} cm^{-1} @ 450 nm, $\Delta\varepsilon \approx 28$ L mol^{-1} cm^{-1} @ 550 nm), the modulation of luminescence cannot be explained by means of radiative energy transfer. In fact, a thin film of the undoped complex with the same thickness has no measurable absorbance in the visible range (see Fig. S5†).

To further investigate this aspect, an additional experiment in which the luminophore and the complex were physically separated was designed. In this way, if the interaction between the luminophore and the complex is basically radiative, the modulation of the luminescence should be still detectable. To this end, we spin-coated a thin film of the undoped complex **1** over a glass slide and an acridine orange doped PMMA film on a Si wafer. The deposition conditions and the concentrations of the complex and luminophore were the same as those employed before. Then, the glass substrate can be used as a physical barrier between the two films by putting it on top of the PMMA sample. After cycling the ensemble under similar conditions as in the previous experiments and in spite of the fact that the luminescence was of the same order of magnitude as those for the doped films, no modulation of the luminescence by the SCO was observed. More detailed studies involving temperature-dependent fluorescence lifetime measurements will be necessary to better understand the quenching mechanism in our system. (This type of measurements may, however, be complicated due to the simultaneous excitation of the luminophore and the complex.)

Nano-dots

In order to go one step further in the observation of the complex at even smaller dimensions, we have developed a soft lithography approach using PDMS stamps[28,29] to create arrays of nanodots from our SCO compound. Micro- and nanometric patterns have

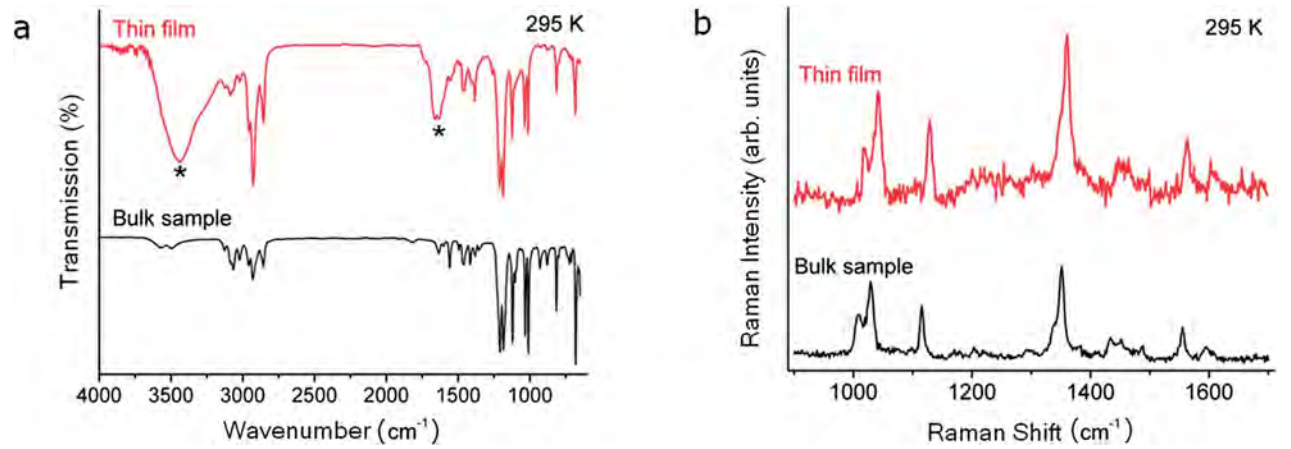

Fig. 1 (a) Infrared spectrum of **1** for a thin film (transmission mode, KBr substrate) and bulk sample (ATR mode). *Water traces found in the KBr substrate. (b) Raman spectra (632.8 nm excitation) of **1** for a thin film and bulk sample.

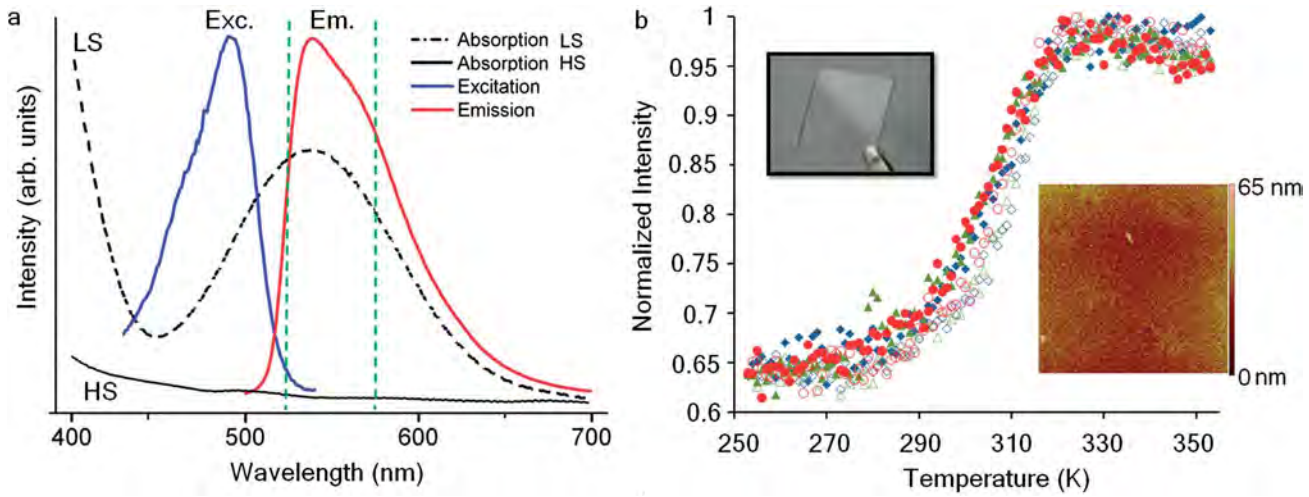

Fig. 2 (a) Normalized excitation and emission spectra of **1** doped with acridine orange in the solid state at room temperature (RT). Blue: excitation spectrum for 560 nm emission; red: emission spectrum for 450 nm excitation; black: absorption spectra of an undoped chloroform solution of **1** at RT (dashed line, LS state) and 320 K (solid line, HS state). Vertical dashed lines depict the spectral pass band used in fluorescence microscopy experiments. (b) Normalized thermal variation of the luminescence intensity at 550 nm with an excitation at 450 nm in a spin coated thin film (~85 nm) of **1** doped with acridine orange during three consecutive thermal cycles ($dT/dt = 2$ K min^{-1}; open and closed symbols for heating and cooling modes, respectively). Insets: photograph of a spin coated SCO thin film on a 1 cm^2 quartz substrate and AFM image (34 × 34 μm^2) of its surface.

been previously reported employing similar approaches for depositing different forms of SCO materials.[16,30,31] A key aspect here to obtain nanometric patterns of the pure complex is the successful solubilization of the complex in an appropriate solvent.

For patterning, 3.5 μl of fresh solution of the complex oligomers in chloroform mixed with acridine orange was spread onto a piece of Si wafer and then, a nano-patterned PDMS stamp was put rapidly on top of the drop and the ensemble was placed into an oven at 353 K for a few minutes. Due to the homogeneous nature of the solution, the moderately high surface tension and high vapor pressure of the chloroform, the solution can easily penetrate into the openings and also evaporate rapidly enough to sweep the excess complex out to the surroundings of the stamp. As a result, nano-droplets of the solution become trapped in the cavities of the PDMS stamp and once the solvent is evaporated, they form nanodots that precipitate in an organized manner onto the Si substrate (Fig. 3). After use, the stamp can be cleaned with ethanol in an ultrasonic bath and be employed for additional patterning processes.

It is important to note that we have been able to build up submicronic motifs in a reproducible way in spite of the important swelling effect that chloroform has when it is in contact with PDMS (swelling ratio = 1.39).[32] We employed thick (around 4 mm thickness) and highly polymerized (rigid) stamps in order to circumvent this problem; due to the small amount of time during which the solvent is in contact with the PDMS before the evaporation, there is no significant or permanent damage of the stamp for several uses. In fact, we believe that this small deformation enhances the adherence of the stamp to the substrate and by the same token the formation of the droplets in the cavities of the stamp.

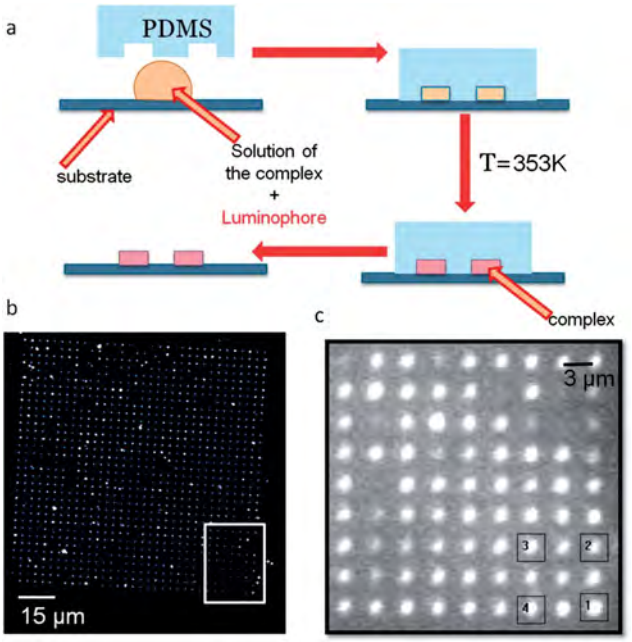

Fig. 3 (a) Scheme of the fabrication process for the arrays of SCO nanodots; (b) dark field image of a nano-dot array obtained with motifs of 370 nm lateral size, 3 µm pitch and a nominal depth of 150 nm; and (c) fluorescence image of the dots in the area highlighted in (b).

The size and shape of the cavities in the PDMS stamps are the two factors that essentially define the geometry of the nanodots. Fig. 4 displays the AFM profiles of a few dots from the lower right corner of the network displayed in Fig. 3c; the height of the dots is fairly uniform with an average value of *ca.* 150 nm that is in agreement with the initial height value of the cavities in the stamp. Alternatively, SEM images (Fig. 5) give a better idea of

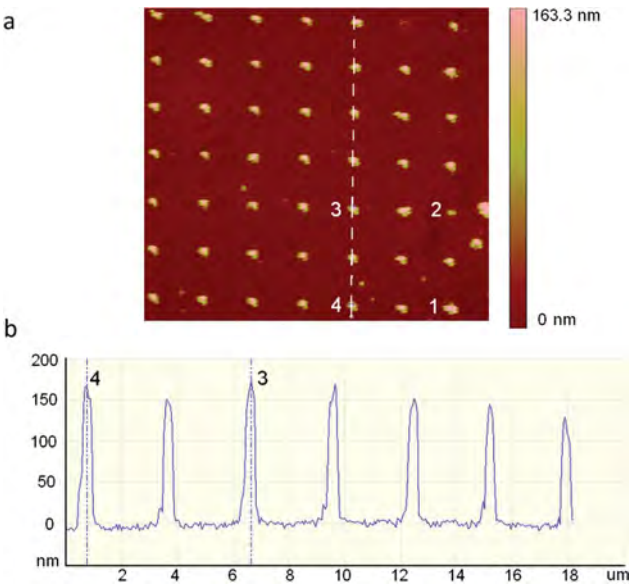

Fig. 4 (a) AFM image (21 × 21 µm²) and (b) a height profile of the luminescent nano-dot array along the dashed line in the area highlighted in Fig. 3b.

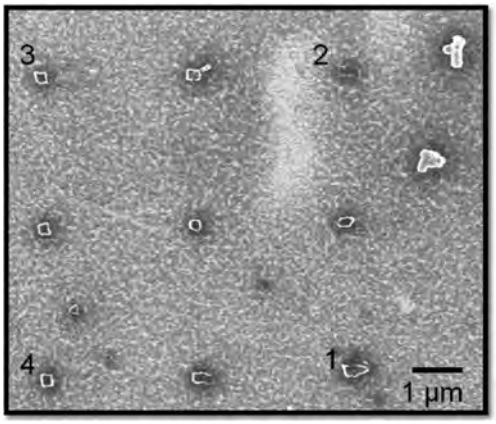

Fig. 5 SEM image of the luminescent array displayed in Fig. 3 and 4. Structures with 200 nm of lateral size are typically observed.

the shape of the same nano-dots; here, it can be seen that the average lateral size of the structures (~200 nm) is less than the nominal size of their respective mold (~370 nm). *A priori*, this could be attributed to a few causes: first, it could be simply that the size of the patterns in the stamp after demolding is smaller; second, the swelling of the PDMS in contact with chloroform reduces the effective volume for trapping the solution and finally, the quantity of complex in solution flowing into the cavities of the stamp is not enough to completely fill them. In fact, we have seen a size reduction effect while varying the lateral size of the motif from 370 nm to 250 nm at a constant complex concentration in the solution; the resulting dimensions of the structure are usually beneath the nominal value of the pattern. (Actually, this observation could be a powerful tool to reach smaller structures beyond the capabilities of the fabrication technique of the Si master.)

The luminescence of the arrays was followed with the same experimental setup employed for the thin film samples except that a higher numerical aperture objective was used in order to improve the signal-to-noise ratio. Due to the thermal dilation of the sample holder, correction of the focus had to be applied every few images. Nonetheless, for making a reliable analysis of the luminescence coming from the sample and due to the large quantity of images that each experiment produces, alignment software under the MATLAB® environment was specifically developed for post-treating the stack of images and compensating automatically any drift of the sample during the experiments.

The most important result is that the fluorescent microscopy images allowed us to follow the variation of the luminescence coming from the individual dots when the temperature is changed (see Movie M1 in the ESI†). As shown in Fig. 3c, the CCD image can be divided into small regions of interest (ROI) each corresponding to a unique dot. Then, by plotting the mean value of the signal against temperature for a given ROI (Fig. 6a), a variation of the luminescence and even a hysteresis can be typically depicted in the same temperature range where the SCO phenomenon is expected to take place (see similar responses of other isolated nano-objects in Fig. S6†). We have been able to detect this type of response also for dots with ~150 nm in lateral size (Fig. 6b) formed from 250 nm PDMS networks (see also

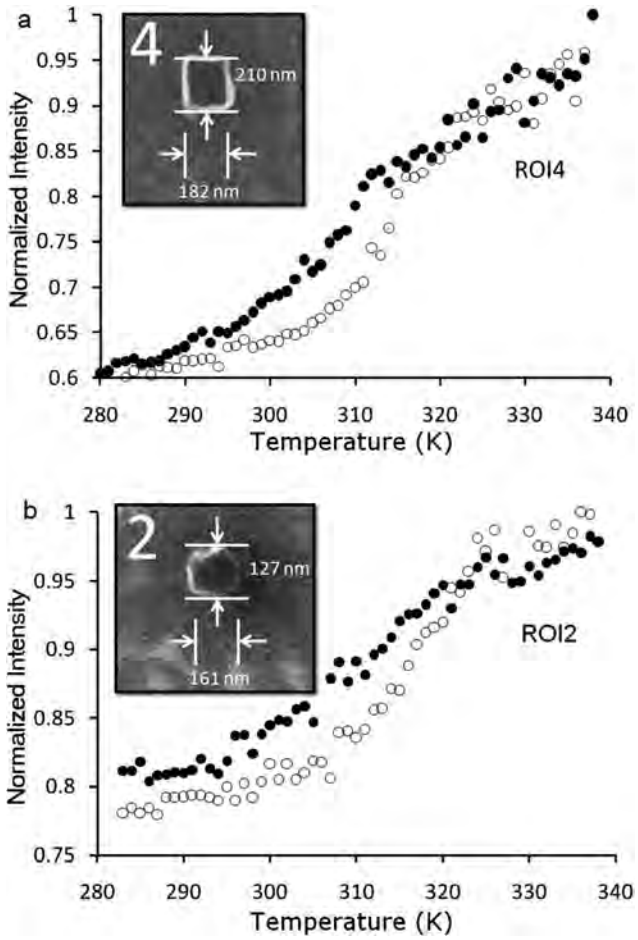

Fig. 6 Normalized thermal variation of the luminescence at 550 nm for (a) nano-dot n°4 from Fig. 3–5, and (b) nano-dot n°2 in the array formed with the motif of 250 nm lateral size and a pitch of 3 μm (see Fig. S7 and S8 in the ESI†). Open and closed symbols indicate heating and cooling modes, respectively. The insets show the magnified SEM images of the nano-dots.

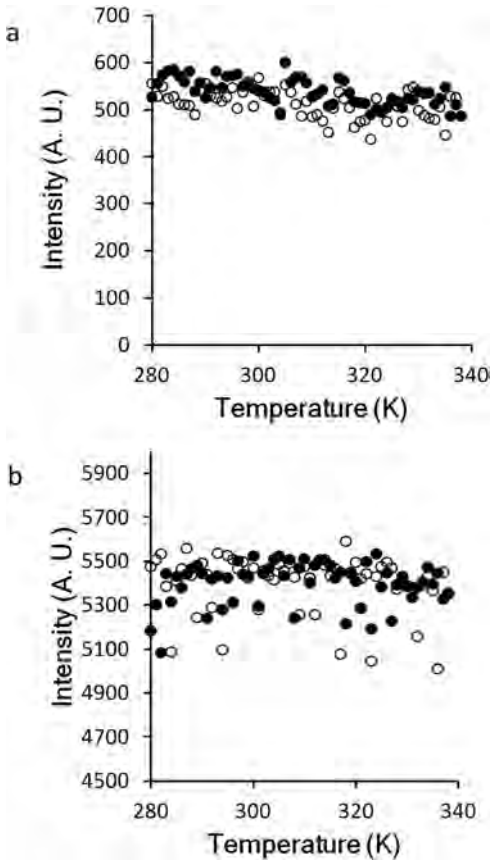

Fig. 7 Thermal variation of the reflected light intensity measured at 543 nm (FWHM = 23 nm) in (a) dark field mode for a nano-dot from an undoped array obtained with a motif of 300 nm lateral size and 2 μm pitch and (b) bright field mode for a nano-dot from an undoped array obtained with a motif of 370 nm lateral size and 2 μm pitch. Open and closed symbols stand for heating and cooling modes, respectively.

Fig. S7 and S8†). The numbers present in each figure that display the array of nano-objects always refer to a specific dot of the ensemble, regardless of the type of imaging technique employed. In consequence, it is possible to associate to each structure its own geometry and specific SCO behavior. Here for the first time, we report a platform and methodology to systematically produce with a controlled size, to organize essentially over any substrate, to characterize morphologically and to monitor in a massively parallel way the SCO phenomenon for a large number of isolated single SCO nano-objects *via* fluorescence microscopy.

To better illustrate the potential of our approach in monitoring SCO at a small scale, undoped versions of these samples were also prepared in order to study them with other optical techniques. We tried—under the same experimental conditions—to perform reflectance measurements (543 nm) for different patterns in bright field and dark field microscopy modes. From these experiments it was impossible to observe any variation that could be attributed to the SCO phenomenon (Fig. 7).

Conclusions

In summary, we have elaborated good quality thin films of the $[Fe(hptrz)_3](OTs)_2$ SCO complex doped with acridine orange. Owing to a radiationless energy transfer process between the low spin Fe(II) ions of the complex and the luminophore, we have been able to follow the spin state changes through luminescence measurements even in thin films at thicknesses below 100 nm. We have also demonstrated the possibility to pattern regular arrays of nano-objects of $[Fe(hptrz)_3](OTs)_2$ using a soft lithography approach and we have been able to monitor the SCO behavior in a large number of widely spaced individual nano-objects simultaneously for sizes down to 150 nm. Even at this small scale, basically similar transition curves have been obtained implying no significant size effect on the SCO in our nano-structures, which is an important asset for future applications. One should note that in our approach there are no surfactants or other stabilizing agents around the nano-objects, hence possible matrix effects are totally discarded. Our method provides a direct way to determine single-particle spin transition curves and the corresponding particle morphologies or even spectral or structural information. Clearly, the limits of the technology employed for fabricating the silicon master or that of the PDMS molding are

not yet reached and the luminescence detection limits can be also easily pushed further. Hence we expect that using this approach one can gain systematic statistical data about the size reduction effects in SCO materials of general relevance to size effects in molecular solids.

These thin films and nano-structures have also a great potential to be used as localized sensors for microthermometry applications.[8,33,34] The key advantage of our luminescent SCO nanomaterials over traditional luminescent thermal imaging is the possibility to fine tune the thermal spin crossover curve, while the optical properties and the luminophore remain unchanged. Another interesting application is related to the fact that the spin crossover is accompanied by a significant change of the dielectric permittivity of the material—leading to a spatially periodic change of the refractive index in our arrays. The resulting stimuli-responsive photonic grating behavior of the $[Fe(hptrz)_3](OTs)_2$ patterns is discussed in the accompanying Part 2.[35]

Acknowledgements

This work was financially supported by the THERMOSPIN project (ANR-10-NANO-012-02) and PRES—Université de Toulouse. The authors are grateful to F. Carcenac (LAAS) for the fabrication of the silicon master.

Notes and references

1 T. Asahi, T. Sugiyama and H. Masuhara, *Acc. Chem. Res.*, 2008, **41**, 1790.
2 Spin Crossover in Transition Metal Compounds I–III, in *Topics in Current Chemistry*, ed. P. Gütlich and H. A. Goodwin, Springer, 2004, pp. 233–235.
3 A. Bousseksou, G. Molnár, L. Salmon and W. Nicolazzi, *Chem. Soc. Rev.*, 2011, **40**, 3313.
4 G. Molnár, S. Cobo, J. A. Real, F. Carcenac, E. Daran, C. Vieu and A. Bousseksou, *Adv. Mater.*, 2007, **19**, 2163.
5 C. Arnaud, T. Forestier, N. Daro, E. Freysz, J.-F. Létard, G. Pauliat and G. Roosen, *Chem. Phys. Lett.*, 2009, **470**, 131.
6 F. Prins, M. Monrabal-Capilla, E. A. Osorio, E. Coronado and H. S. J. van der Zant, *Adv. Mater.*, 2011, **23**, 1545.
7 W. E. Moerner and D. P. Fromm, *Rev. Sci. Instrum.*, 2003, **74**, 3597.
8 L. Salmon, G. Molnár, D. Zitouni, C. Quintero, C. Bergaud, J.-C. Micheaud and A. Bousseksou, *J. Mater. Chem.*, 2010, **20**, 5499.
9 S. Titos-Padilla, J. M. Herrera, X.-W. Chen, J. J. Delgado and E. Colacio, *Angew. Chem., Int. Ed.*, 2011, **50**, 3290.
10 Y. Garcia, F. Robert, A. D. Naik, G. Zhou, B. Tinant, K. Robeyns, S. Michotte and L. Piraux, *J. Am. Chem. Soc.*, 2011, **133**, 15850.
11 R. C. Powell and G. Blasse, in *Structure and Bonding*, Springer-Verlag, Berlin, Heidelberg, New York, 1980, vol. 42, ch. 2, pp. 4–96.
12 O. Roubeau, J. M. A. Gomez, E. Balskus, J. J. A. Kolnaar, J. G. Haasnoot and J. Reedijk, *New J. Chem.*, 2001, **25**, 144.
13 A. Grosjean, N. Daro, B. Kauffmann, A. Kaiba, J.-F. Létard and P. Guionneau, *Chem. Commun.*, 2011, **47**, 12382.
14 *US Pat.*, 3821376, 1974.
15 *Inorganic Syntheses*, ed. D. Coucouvanis, John Wiley & Sons, Inc., New York, USA, 2002, vol. 33, ch. 2, p. 91.
16 C. Thibault, G. Molnár, L. Salmon, A. Bousseksou and C. Vieu, *Langmuir*, 2010, **26**, 1557.
17 D. Wang and H. Möhwald, *J. Mater. Chem.*, 2004, **14**, 459.
18 P. T. Hammond, *Adv. Mater.*, 2004, **16**, 1271.
19 S. Cobo, G. Molnár, J. A. Real and A. Bousseksou, *Angew. Chem., Int. Ed.*, 2006, **46**, 5786.
20 M. Seredyuk, A. B. Gaspar, V. Ksenofontov, S. Reiman, Y. Galyametdinov, E. Haase, W. Rentschler and P. Gütlich, *Chem. Mater.*, 2006, **18**, 2513.
21 K. Kuroiwa, T. Shibata, S. Sasaki, M. Ohba, A. Takahara, T. Kunitake and N. Kimizuka, *J. Polym. Sci., Part A: Polym. Chem.*, 2006, **44**, 5192.
22 M. Ruben, J. Rojo, F. J. R. Salguero, L. H. Uppadine and J. M. Lehn, *Angew. Chem., Int. Ed.*, 2004, **43**, 3644.
23 S.-W. Lee, J.-W. Lee, S.-H. Jeong, I.-W. Park, Y.-M. Kim and J.-I. Jin, *Synth. Met.*, 2004, **142**, 243.
24 A. Nakamoto, Y. Ono, N. Kojima, D. Matsumura and T. Yokoyama, *Chem. Lett.*, 2003, **32**, 336.
25 A. Nakamoto, Y. Ono, N. Kojima, D. Matsumura and T. Yokoyama, *Chem. Lett.*, 2003, **32**, 476.
26 H. Soyer, C. Mingotaud, M.-L. Boillot and P. Delhaes, *Langmuir*, 1998, **14**, 5890.
27 G. Félix, K. Abdul-Kader, T. Mahfoud, I. A. Gural'skiy, W. Nicolazzi, L. Salmon, G. Molnár and A. Bousseksou, *J. Am. Chem. Soc.*, 2011, **133**, 15342.
28 Y. Xia and G. M. Whitesides, *Annu. Rev. Mater. Sci.*, 1998, **28**, 153.
29 B. K. Gale, M. A. Eddings, S. O. Sundberg, A. Hatch, J. Kim and T. Ho, in *Comprehensive Microsystems*, Elsevier, Amsterdam, Netherlands, 2008, vol. 1, pp. 341–378.
30 M. Cavallini, I. Bergenti, S. Milita, G. Ruani, I. Salitros, Z.-R. Qu, R. Chandrasekar and M. Ruben, *Angew. Chem., Int. Ed.*, 2008, **47**, 8596.
31 M. Cavallini, I. Bergenti, S. Milita, J. C. Kengne, D. Gentili, G. Ruani, I. Salitros, V. Meded and M. Ruben, *Langmuir*, 2011, **27**, 4076.
32 J. N. Lee, C. Park and G. M. Whitesides, *Anal. Chem.*, 2003, **75**, 6544.
33 P. Löw, B. Kim, N. Takama and C. Bergaud, *Small*, 2008, **4**, 908.
34 J. Lee and N. A. Kotov, *Nano Today*, 2007, **2**, 48.
35 A. Akou, I. A. Gural'skiy, L. Salmon, C. Bartual-Murgui, C. Thibault, C. Vieu, G. Molnár and A. Bousseksou, *J. Mater. Chem.*, 2012, DOI: 10.1039/C2JM15663F.